Journal of MATERIALS RESEARCH

Article
DOI:10.1557/s43578-022-00864-z

Theoretical investigations of structural, electronic, optical and elastic properties of wurtzite $ZnO_{1-x}Se_x$ ternary alloys using first principle method

Yacine Djalab[1], Rabah Moussa[1,a)], Mostefa Maache[2], Syed Awais Rouf[3], Ahmed Abdiche[4], Rabah Khenata[4], Fethi Soyalp[5]

[1] Physics Department, Physico-Chemistry of Materials and Environment Laboratory, Ziane Achour University of Djelfa, BP 3117, Djelfa, Algeria
[2] Physics Department, FECS, Ziane Achour University, 17 000, Djelfa, Algeria
[3] Department of Physics, Division of Science and Technology, University of Education, Lahore, Pakistan
[4] Laboratoire de Physique Quantique de la Matière et de Modélisation Mathématique (LPQ3M), Université de Mascara, 29000 Mascara, Algerie
[5] Department of Physics, Faculty of Education, Yüzüncü Yil University, 65080 Van, Turkey
[a)] Address all correspondence to this author. e-mail: moussa.rabah@univ-djelfa.dz

Received: 28 September 2022; accepted: 5 December 2022

We have explored the structural, electronic, optical, and elastic properties of $ZnO_{1-x}Se_x$ ($x = 0$, 0.25, 0.50, 0.75 and 1) ternary alloys with wurtzite structure (WZ). We have used the full potential linearized augmented plane wave method in the framework of density functional theory. The lattice parameters, bulk modulus, and first pressure derivative are determined in the WZ phase using the equation of state of Birch–Murnaghan. The variations of structural parameters versus the concentration *x* deviate slightly from Vegard's law. The electronic properties including bandgap energy, are studied for ternary alloys with their binary constituents, and the studied materials fall in the domain of direct bandgap semiconductors. Moreover, the optical properties like dielectric function, refractive index, reflectivity and absorption coefficient are examined. The findings of this works could be worthful for the development and preparation of these materials for wide-range of optoelectronic applications.

Introduction

Group II–VI semiconductors have attracted considerable interests of scientists across the world owing to their potential to replace the group III–V semiconductors in diversity of applications particularly optoelectronic industries. Due to their large bandgap, these semiconductors are auspicious in the fabrication of optoelectronic devices that operate in the blue to near ultraviolet (UV) range. Among these compounds, zinc oxide (ZnO) is a notable semiconductor. Its wide direct bandgap and large exciton binding energy make it a good candidate for optoelectronic applications such as high-mobility low-temperature transistors, photodetectors, transparent conducting films, UV light emitters, sensors, etc. [1–10]. It is necessary to tune the ZnO bandgap to account for both ultraviolet and visible light emissions. As a result, efforts are being made to engineer the bandgap of ZnO-based materials.

Alloying is a commonly used process for engineering the bandgap of semiconductor materials to meet the needs of desired applications. For instance, the substitution of zinc (Zn) by magnesium (Mg) has been employed; the ternary alloy Mg_xZnO_{1-x} exhibits an increase in bandgap with the increase in Mg contents [11, 12]. The elaboration and characterization of $Cd_yZn_{1-y}O$ ternary alloy shows that its bandgap energy decrease with increase in cadmium (Cd) concentration which makes this ternary alloy very suitable for optical and solar cell applications [11, 13]. However, cadmium is a toxic substance; thus, it is necessary to find the alternate materials. One of these materials is selenide (Se). The $ZnO_{1-x}Se_x$ alloy belongs to a class of semiconductors known as highly mismatched alloys (HMAs). The substitution of O with selenide Se atoms that are considerably bigger and less electronegative than O atoms, results in a perturbation of the band structure. It is difficult to synthesize such HMAs owing to the difference in atomic size and electronegativity. The energy band structure of these HMAs is determined by an anticrossing interaction between the localized states of minority and extended band states of majority components of the alloys.

Numerous theoretical studies on $ZnO_{1-x}Se_x$ alloy have been reported [14–16]. The influence of selenide atomic concentrations on structural and optical properties of ternary $ZnO_{1-x}Se_x$ alloys have been investigated using the DFT method implemented in the VASP package, as well as the partially self-consistent scGW$_0$ approach [15]. The variations in lattice constants as a function of selenide concentration deviate by 0.5% from Vegard's law. Moreover, a large absorption coefficient is observed in low energy area. The findings show that the bandgap of $ZnO_{1-x}Se_x$ ternary alloy can be tuned to a desired value suitable for solar cell and energy applications.

The ternary alloys $ZnO_{1-x}Se_x$ have been grown experimentally through radical source molecular beam epitaxy (RS-MBE) [17]. Whereas, using the pulsed laser deposition technique (PLD), $ZnO_{1-x}Se_x$ films with various selenium concentrations have also been deposited on the sapphire substrate (001). The thin films possess a single phase; the hexagonal wurtzite structure with preferred c-axis orientation. Various studies have reported the attempts to engineer the bandgap of the $ZnO_{1-x}Se_x$ alloys [18–23]. For example, Mayer et al. [20] synthesized $ZnO_{1-x}Se_x$ alloys with Se substitutional composition $x<0.12$ using pulsed laser deposition. In this study, the bandgap energy was successfully reduced to 2.05 eV. Current study aims to calculate the structural, electronic, and optical properties as well as elastic properties of the ternary $ZnO_{1-x}Se_x$ alloy with wurtzite structure. This study paves the pathways for experimental assembly of these materials with enhanced and controlled characteristics for the desired optoelectronic applications.

Results and discussion

Structural properties

The wurtzite structure can be described by three parameters a, c and u (internal parameter). All these parameters have been calculated for the lowest energy of the crystal. The lattice constants, bulk modulus B_0 and its first pressure derivative B' have been optimized by fitting the obtained total energy as a function of volume to Birch-Murnaghan's equation of state [24]. The total energy versus volume for different values of Se concentration has been plotted in Fig. 1. The structural properties of $ZnO_{1-x}Se_x$ ternary alloys and their binary compounds ZnO and ZnSe are given in Table 1**.** The calculations with WC-GGA scheme give the values of a as 3.24, c as 5.19 and c/a as 1.60 for wurtzite ZnO, and a as 3.99, c as 6.46 and c/a as 1.62 for ZnSe. These values agree well with the experimental and theoretical reports available in literature. For the ternary alloys, the values of lattice parameters a and c increase with the increase in concentration of Se, however, their ratio (c/a) remains the same. The obtained values have also been compared with that reported in Ref. [15]. The variation trends of a and c with change in x are shown in Fig. 2. According to Vegard's law [33], the lattice parameters for wurtzite $ZnO_{1-x}Se_x$ ternary alloys as a function of composition x can be explained in terms of their binary components ZnO and ZnSe using the following equations:

$$a_{\text{alloy}}(x) = (1-x)a_{\text{ZnO}} + xa_{\text{ZnSe}} \quad (1)$$

$$c_{\text{alloy}}(x) = (1-x)c_{\text{ZnO}} + xc_{\text{ZnSe}} \quad (2)$$

where a_{alloy} and c_{alloy} are the lattice constants of the ternary alloy, and a_{ZnO}, c_{ZnO}, a_{ZnSe} and c_{ZnSe} are the lattice parameters of binary compounds, respectively. Figure 2 shows that the curves for a and c deviate from Vegard's law and obey to the following quadratic equations:

$$a_{\text{alloy}}(x) = (1-x)a_{\text{ZnO}} + xa_{\text{ZnSe}} - x(1-x)b \quad (3)$$

$$c_{\text{alloy}}(x) = (1-x)c_{\text{ZnO}} + xc_{\text{ZnSe}} - x(1-x)b \quad (4)$$

where b is the bowing parameter. It is found that the downward bowing parameter is equal to − 0.29 and − 0.62 for a_{alloy} and c_{alloy}, respectively. Furthermore, this deviation can be explained by lattice mismatch between the ternary alloy and its binary constituents, ZnO and ZnSe.

Electronic properties

Band structure

The electronic band structure is fundamental in the study of electronic properties of semiconductors, and its knowledge is crucial in the fabrication of various optoelectronic devices. Electronic band structure of $ZnO_{1-x}Se_x$ ternary alloys with their binary compounds ZnO and ZnSe are computed using the TB-mBJ approach as shown in Fig. 3. The valence band maxima (VBM) and conduction band minima (CBM) in each band structure are located in the same symmetry point Γ which clearly indicates that the studied materials are direct bandgap semiconductors. The bandgap energy of these alloys is investigated using both PBE-GGA and TB-mBJ approximations, and their results are summarized in Table 2. The bandgap energy computed with TB-mBJ approach is substantial ameliorated compared to that obtained through PBE-GGA approximation. The experimental and theoretical values of energy bandgap reported for ZnO and ZnSe are given in Ref. [15]**.** These values are smaller than that of calculated by TB-mBJ approach.

The evolution of energy bandgap as a function of x as calculated by PBE-GGA and TB-mBJ approximations is depicted in Fig. 4. It is obvious from figure that the bandgap energy decrease with the increase in x before to 0.5, and then increases with the increase in x. The variations in bandgap energy with change in x can be well explained by the following quadratic formula [36]:

$$E_g(x) = xE_{g,\text{ZnSe}} + (1-x)E_{g,\text{ZnO}} - x(1-x)b \quad (5)$$

where $E_g(x)$, $E_{g,\text{ZnSe}}$ and $E_{g,ZnO}$ denote the bandgap of $ZnO_{1-x}Se_x$, ZnO and ZnSe, respectively. The deviation of bandgap from

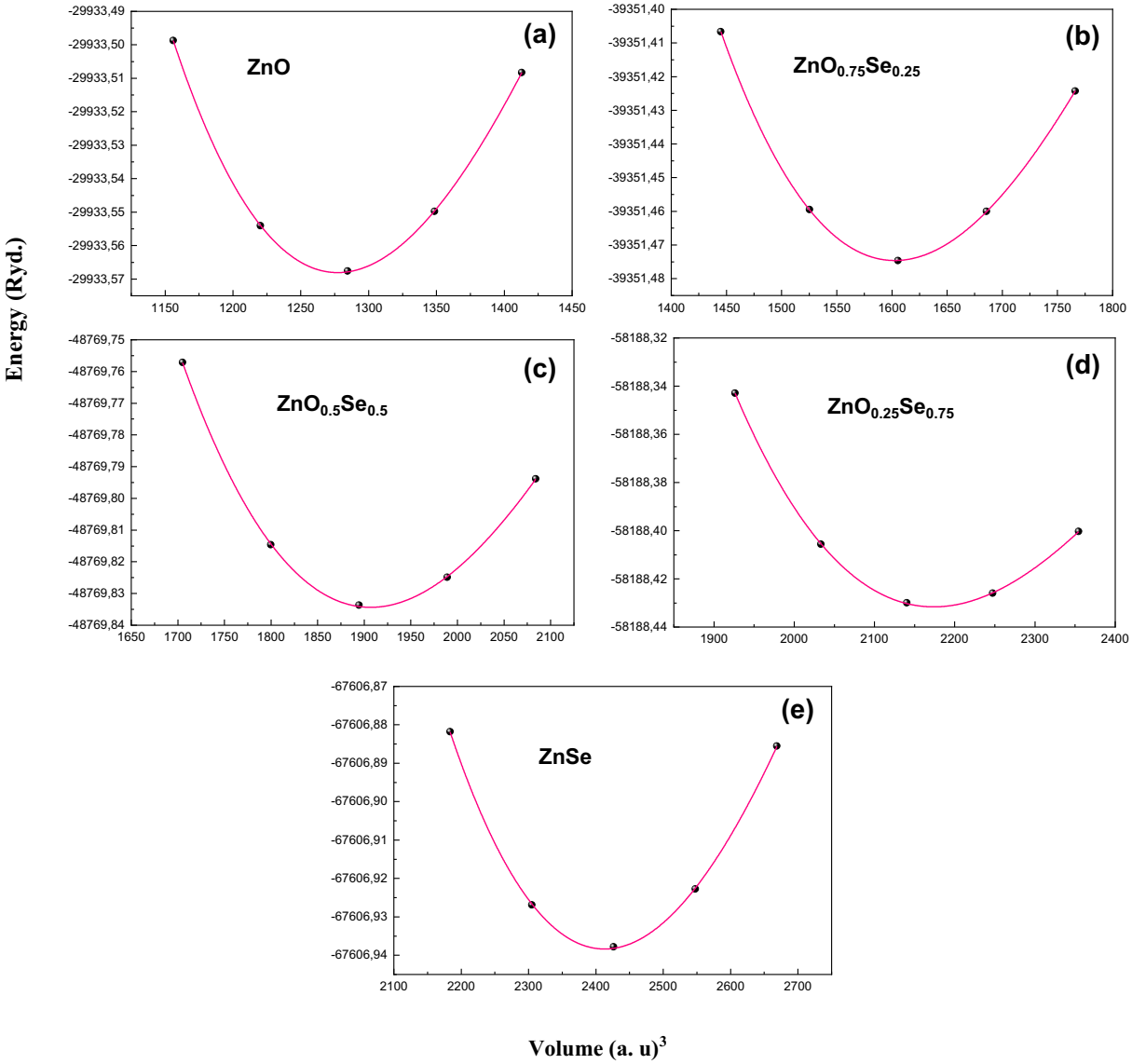

Figure 1: (a–e) Total energy versus the volume curves of the wurtzite $ZnO_{1-x}Se_x$ ternary alloys.

linear composition dependency can be described with the help of bowing parameter b. The bandgap energy variations obtained using the PBE-GGA and TB-mBJ approximations are governed by the following equations:

$$E(x)_{\mathrm{g}}^{\mathrm{TB\text{-}mBJ}} = 2.86x + 2.68(1-x) + 0.85x(1-x) \quad (6)$$

$$E(x)_{\mathrm{g}}^{\mathrm{PBE\text{-}GGA}} = 1.39x + 0.82(1-x) + 0.96x(1-x) \quad (7)$$

The energy bandgap curves against change in x of these alloys show an upward bowing parameter of 0.85 ± 0.2 eV and 0.96 ± 0.2 eV as calculated from PBE-GGA and TB-mBJ approximations, respectively. These values of bowing parameter are attributed to difference in electronegativity of O (3.44) and Se (2.55).

Moreover, the bowing parameter b is originally divided into tree physical contributions; the first term is volume deformation representing the relative response of the binary constituents ZnO with ZnSe to hydrostatic pressure between the equilibrium lattice constants from these binary compounds to their ternary alloy. The second one is charge exchange contribution described by charge transfer in bringing ZnO and ZnSe compounds to the ZnOSe alloy. The last term is the structural relaxation due to the change of the bandgap upon passing from the unrelaxed to the relaxed alloy [37].

The density of states

The computed total density of states (TDOS) and partial density of states (PDOS) of ZnO and ZnSe as well as the ternary alloy

TABLE 1: The calculated equilibrium parameters such as lattice constants *a* and *c*, bulk modulus *B* and its pressure derivative *B′* of the wurtzite $ZnO_{1-x}Se_x$ ternary alloy.

$ZnO_{1-x}Se_x$		This work using WC-GGA					
		a (Å)	c (Å)	c/a	u	B	B′
ZnO	Pres	3.24	5.19	1.60	0.3807	146.12	4.67
	Theo	3.29[d], 3.286[e], 3.17[f]	5.269[d], 5.269[e], 5.12[f]	1.602[d], 1.603[e]	0.38089[d], 0.38[e]	128.72[e]	4.38[e]
	Exp	3.249[a], 3.249[b]	5.206[a], 5.204[b]	1.601[b]	0.382[c]	183[b], 181[c]	4.0[b], 4.0[c]
$ZnO_{0.75}Se_{0.25}$	Pres	3.48	5.63	1.62	0.37856	105.58	4.54
	Theo	3.34[f]	5.42[f]	–	–	–	–
	Exp	–	–	–	–	–	–
$ZnO_{0.5}Se_{0.5}$	Pres	3.68	5.99	1.62	0.37658	85.06	4.61
	Theo	3.53[f]	5.75[f]	–	–	–	–
	Exp	–	–	–	–	–	–
$ZnO_{0.25}Se_{0.75}$	Pres	3.85	6.24	1.62	0.37695	71.90	4.75
	Theo	3.74[f]	6.11[f]	–	–	–	–
	Exp	–	–	–	–	–	–
ZnSe	Pres	3.99	6.46	1.62	0.37406	65.80	3.41
	Theo	3.93[h] 4.043[i], 3.93[f]	6.464[h], 6.703[i], 6.44[f]	1.64[h]	0.3740[h], 0.371[i]	70.78[h]	4.73[h]
	Exp	3.996[g]	6.626[g]	–	0.375[g]	–	–

[a][25].
[b][26].
[c][27].
[d][28].
[e][29].
[f][15].
[g][30].
[h][31].
[i][32].

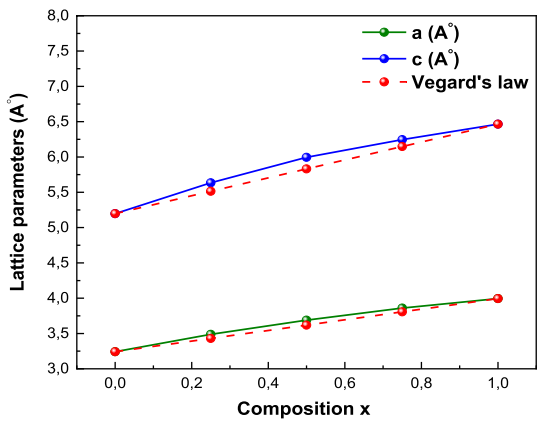

Figure 2: Lattice parameters *a* and *c;* as a function of composition *x* for the wurtzite $ZnO_{1-x}Se_x$ ternary alloy.

$ZnO_{0.75}Se_{0.25}$ are shown in Fig. 5. There are three distinct regions in the TDOS spectrum: the lower valence band (LVB), the upper valence band (UVB), and the conduction band (CB). For ZnO, the DOS is shown in Fig. 5(a). The LVB is essentially dominated by O-2*s* states with a few contributions of Zn-3*p* states. Whereas, the UVB is mainly formed by Zn-3*d* and O-2*p* states with a small contribution os Zn-3*p*-4*s* states. The CB is created by the combined contribution of Zn-4*s*-3*p* states with a few participations of O-2*p* states.

The TDOS and PDOS of ZnSe are depicted in Fig. 5(b). The LVB is formed by the contribution of Se-4*s* states with a small contribution of Zn-4*s*-3*p* states, and the UVB is dominated by the Zn-3*d* states with a small contribution of the Zn-4*s* and Se-4*p* states. The CB region is essentially formed by the contributions of Zn-4*s*-3*p* states with a small participation of Se-4*p*-3*d* states.

Furthermore, for both ZnO and ZnSe binary compounds, there is large contribution of Zn-3*d*, O-2*s* and Se-4*s* states to the valence band, while the Zn-4*s* states contribute to the formation of the conduction band, these compounds exhibit semiconducting nature with a distinctive bandgap up the Fermi level. Therefore Zn-3*d* states are broadened between − 3 eV and − 6 eV and according to the photoemission results, the Zn-3*d* state could be situated at about − 6 eV in the valence band [38]. The experimental work of Girard with co-authors [39] gives more detail about Zn-3*d* states position in the valence band of the ZnO compound in the wurtzite phase.

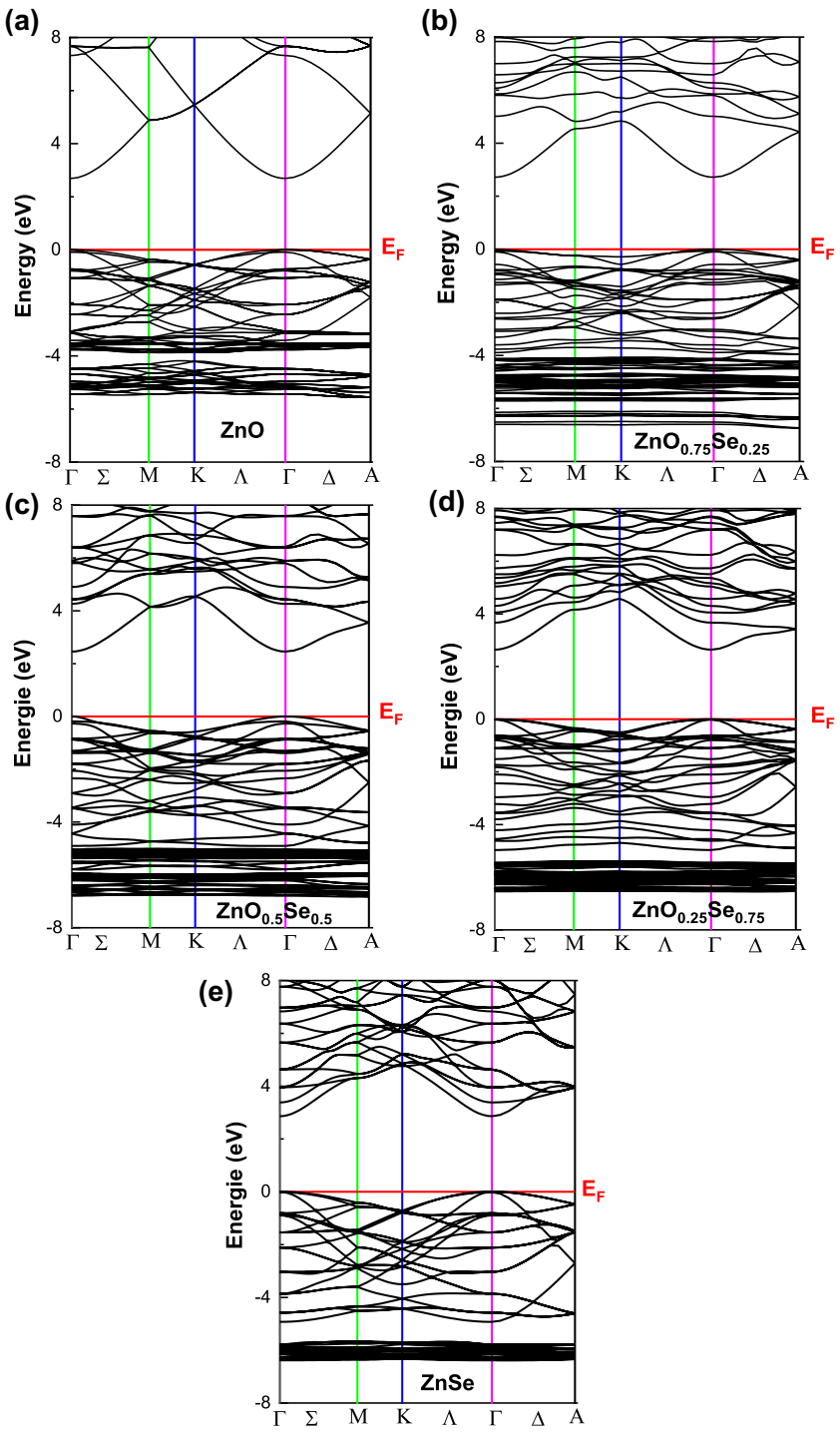

Figure 3: (a–e) Band gap energies of the wutrzite $ZnO_{1-x}Se_x$ ternary alloys.

For $ZnO_{0.75}Se_{0.25}$ alloy that we have chosen as prototype, the DOS is plotted in Fig. 5(c) which shows that the LVB is formed by the contribution of O-2*s* and Se-4*s* states. The UVB is dominated by the participation of Zn-4*s*-3*p* states with a small contribution of O-2*p* and Se-4*p* states. The CB is formed by the mixture contribution of Zn-4*s*-3*p*, O-2*p* and Se-4*p*-3*d* states.

Optical properties

The optical properties allow us to understand the interaction of light with matter. These properties are strongly correlated with the electronic properties, especially the bandgap. We can describe the response of any material to electromagnetic radiation by knowing its complex dielectric function [$\varepsilon(\omega)=\varepsilon_1(\omega)+i\varepsilon_2(\omega)$]. The imaginary part

TABLE 2: The direct band gap energies $E_{\Gamma\to\Gamma}$ (eV) of the (WZ) $ZnO_{1-x}Se_x$ ternary alloys.

$ZnO_{1-x}Se_x$	Band gaps	PBE-GGA	TB-mBJ	Other works
ZnO	$E_{\Gamma\to\Gamma}$	0.82	2.68	3.44[a]
$ZnO_{0.75}Se_{0.25}$	$E_{\Gamma\to\Gamma}$	0.90	2.71	1.64[b]
$ZnO_{0.5}Se_{0.5}$	$E_{\Gamma\to\Gamma}$	0.75	2.45	1.46[b], 1.73[b]
$ZnO_{0.25}Se_{0.75}$	$E_{\Gamma\to\Gamma}$	1.10	2.64	1.86[b]
ZnSe	$E_{\Gamma\to\Gamma}$	1.39	2.86	2.71[c]

[a][34].

[b][15].

[c][35].

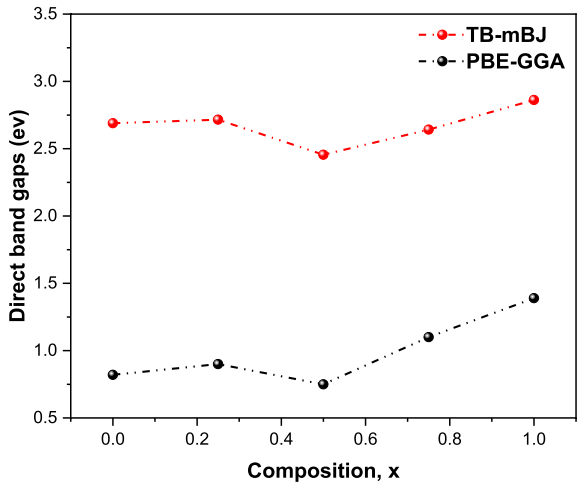

Figure 4: Direct band gaps energies as function of the composition of the $ZnO_{1-x}Se_x$ ternary alloys.

of dielectric function is equivalent to the sum of all possible transitions between occupied and unoccupied states. It is also closely related to the band structure of the material. Following formula is used to determine the imaginary part of dielectric function $\varepsilon_2(\omega)$ [40]:

$$\varepsilon_2(\omega) = \frac{e^2\hbar}{\pi m^2\omega^2}\sum_{v,c}\int_{BZ}|M_{cv}(k)|^2[\omega_{cv}(k)-\omega]d^3 \quad (8)$$

The integral is across the first Brillouin zone and $M_{cv}(k)$ is the momentum dipole elements which is given as:

$$M_{cv}(k) = u_{ck}|e\nabla|u_{vk} \quad (9)$$

The real part of dielectric function $\varepsilon_1(\omega)$ is related to the imaginary part through well-known Kronig relation [41]:

$$\varepsilon_1(\omega) = 1 + \frac{2}{\pi}P\int_0^\infty \frac{\omega'\varepsilon_2(\omega')}{\omega'^2-\omega^2}d\omega' \quad (10)$$

where P represents the principal value of the integral. The information of real and imaginary components of the dielectric function enable us to compute the other important optical functions including refractive index [42]:

$$n(\omega) = \left[\frac{\varepsilon_1(\omega)}{2} + \frac{\sqrt{\varepsilon_1^2(\omega)+\varepsilon_2^2(\omega)}}{2}\right]^{\frac{1}{2}} \quad (11)$$

At low frequency ($\omega=0$), the refractive index becomes:

$$n(0) = \varepsilon^{1/2}(\omega) \quad (12)$$

The reflectivity can be deduced from the following formula:

$$R(\omega) = \left|\frac{\sqrt{\varepsilon(\omega)}-1}{\sqrt{\varepsilon(\omega)}+1}\right|^2 \quad (13)$$

The absorption coefficient is explained in term of real and imaginary parts of the dielectric function as:

$$\alpha(\omega) = \sqrt{2\omega}\left[\sqrt{\varepsilon_1^2(\omega)+\varepsilon_2^2(\omega)}-\varepsilon_1(\omega)\right]^{\frac{1}{2}} \quad (14)$$

The optical properties of ternary alloys and their binary constituents ZnO and ZnSe have been calculated, and the obtained results are shown in Fig. 6(a)–(e). The curves for real part of dielectric function of $ZnO_{1-x}Se_x$ with their binary compounds ZnO and ZnSe are depicted in Fig. 6(a). It is obvious that the value of dielectric function is increased with increase in photon energy over the region 5.0–8.7 eV. Since that increase happened in an area with no absorption, we say that there is a normal dispersion. Afterward, the value of dielectric function decreases with increase in photon energy in the same region, indicating the anomalous dispersion, which is the dispersion that describes the decrease of dielectric function in an absorption band. As the composition 'x' is gradually increased from 0 to 1, the real part of dielectric function is shifted toward the lower photon energy with an augmentation in their amplitudes. However, when the photon energy becomes zero, the values of dielectric constant of the samples is decreased, as tabulated in Table 3.

Figure 6b shows the variation in imaginary part of dielectric function $\varepsilon_2(\omega)$ as a function of photon energy for ternary alloys and their binary components ZnO and ZnSe. $\varepsilon_2(\omega)$ is strongly related to the absorption of materials. One can clearly see that the $\varepsilon_2(\omega)$ curves have major peaks between the two small humps. The value of $\varepsilon_2(\omega)$ increases with increase in photon energy until the major peaks are obtained at 12.66, 9.56, 6.54, 6.19 and 5.7 eV for respective change in x as 0, 0.25, 0.50, 0.75 and 1. The right small humps are located at 15.19, 12.09, 7.82, 7.76 and 7.11 eV for the same respective aforementioned concentrations. Afterward, the value of $\varepsilon_2(\omega)$ decreases with increase in photon energy. Moreover, the left small humps are found at 5.12, 3.44, 4.83 and 4.88 eV for x as 0, 0.25, 0.50 and 0.75, respectively. These humps disappear in case of ZnSe. It is observed that the curves of imaginary part of dielectric function shift toward the lower energy with gradual increase in x.

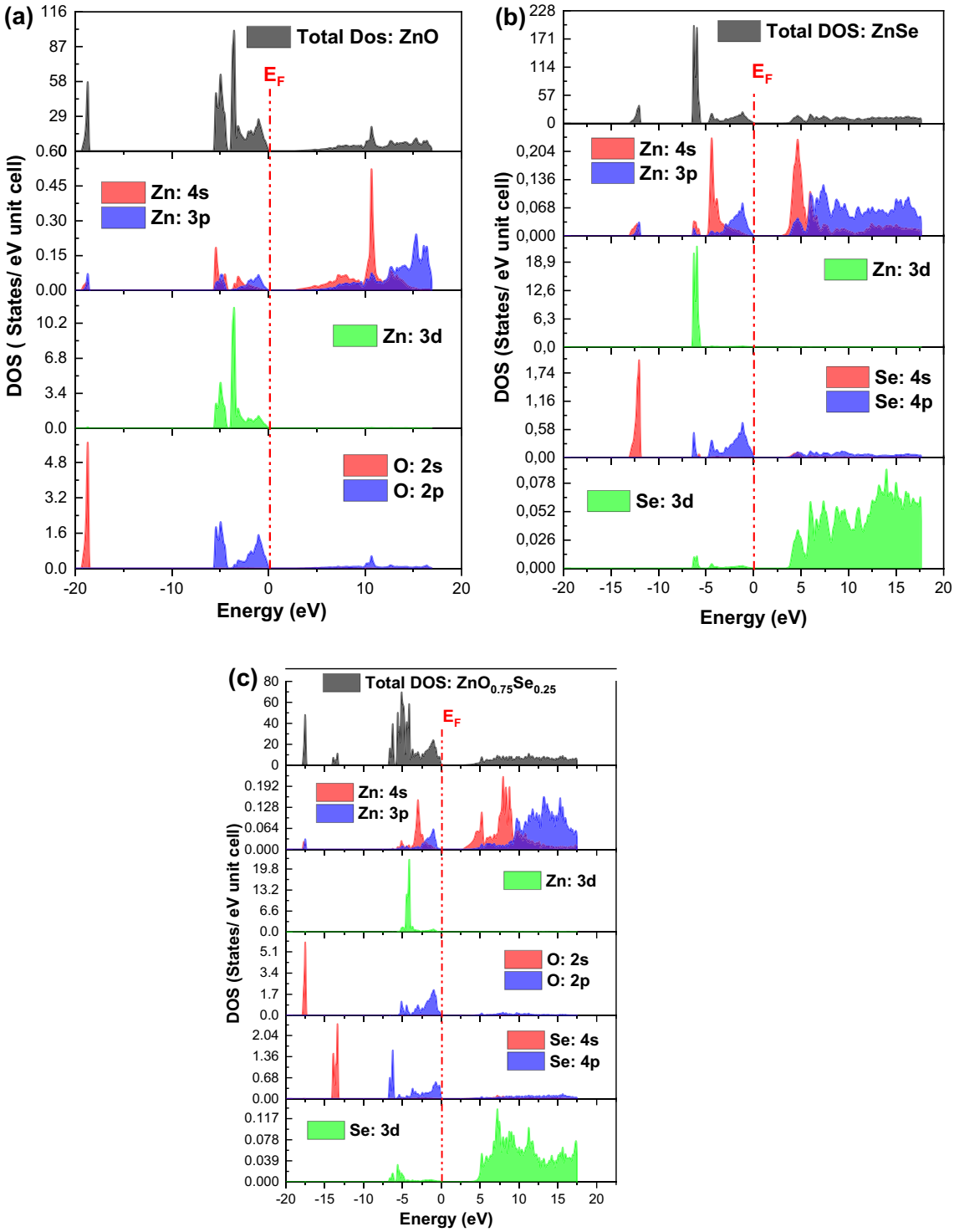

Figure 5: (a–c) Total and partial DOS of the compounds ZnO, ZnSe and $ZnO_{0.75}Se_{0.25}$ alloy as a function of photon energy.

The refractive index is an important property for optoelectronic applications as it is directly associated with the bandgap of the material. Figure 6c shows the refractive index $n(\omega)$ of ternary alloys with binary compounds as a function of photon energy. It has major peaks at 11.66, 5.91, 5.26, 5.89 and 5.21 eV corresponding to the amplitude of 1.97, 2.27, 2.76, 2.95 and 3.33 for the values of x as 0, 0.25, 0.50, 0.75 and 1, respectively. In start, the value of refractive index is increased with increase in photon energy. As the photon energy tends to zero, the refractive index of alloys and compounds are determined by the intercepts of curves with Y-axe, as given in Table 3.

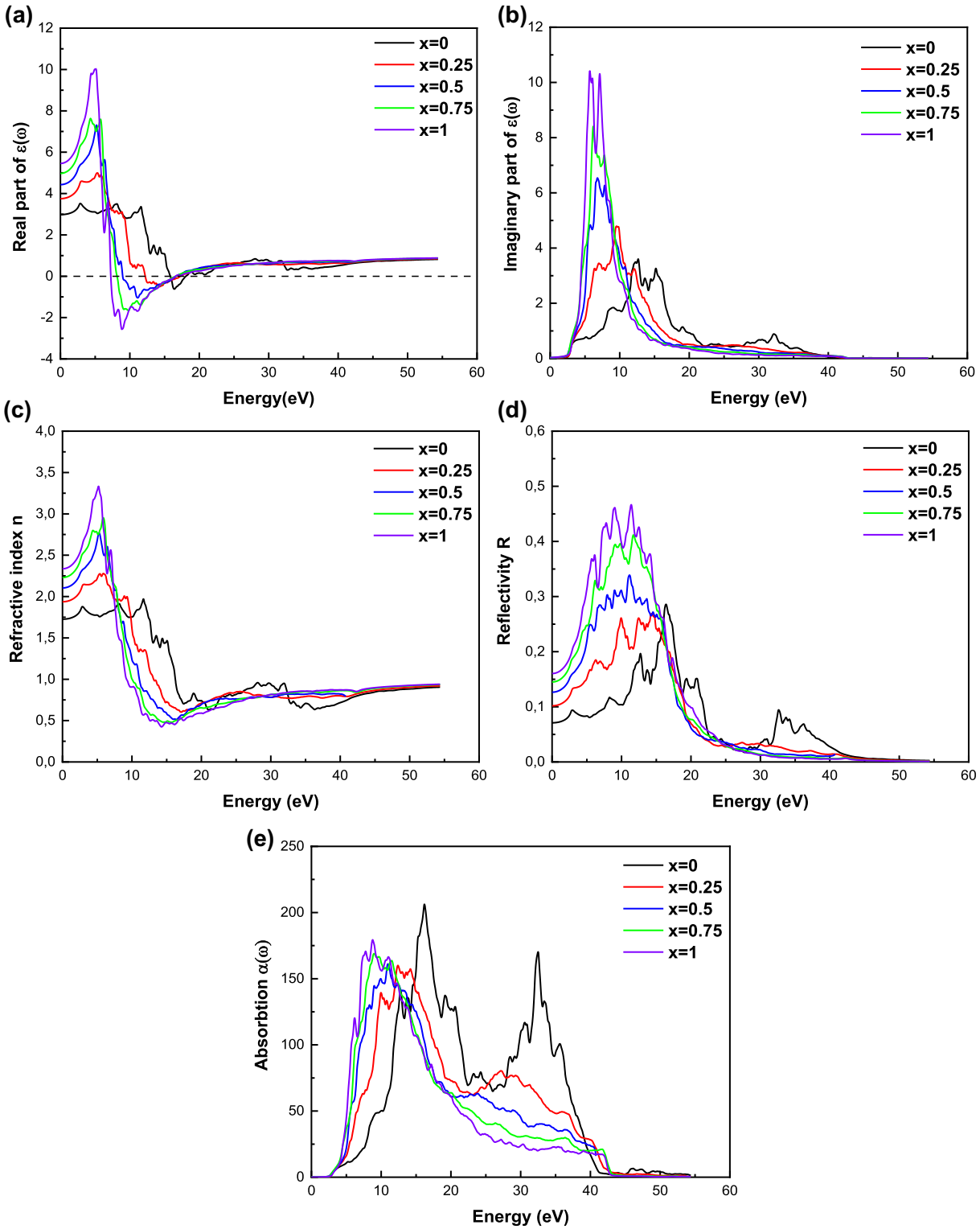

Figure 6: (a–e) Optical parameter spectrums as a function of photon energy for the (WZ) $ZnO_{1-x}Se_x$ ternary alloy; (a) real parts, (b) imaginary parts, (c) refractive indices, (d) reflectivity indices and (e) absorption coefficients.

Figure 6d illustrates the frequency-dependent reflectivity $R(\omega)$ of $ZnO_{1-x}Se_x$ alloys including ZnO, and ZnSe. The value of reflectivity increases with increase in photon energy and its major peaks are observed at 16.44, 14.38, 11.08, 11.74 and 11.38 eV for composition x as 0, 0.25, 0.50, 0.75 and 1, respectively. There appeared a few humps in left region of the principal peak; whereas in right

region, the reflectivity decreased as the photon energy is increased. At zero energy, the reflectivity values are found to be 7.09, 10.18, 12.65, 14.51, and 16.04% for composition x as 0, 0.25, 0.50, 0.75 and 1, respectively. It is concluded that the reflectivity of the studied materials is increased by ~ 2% with increase in x from 0 to 1.

The absorption coefficient $\alpha(\omega)$ profiles of proposed alloys and compounds are presented in Fig. 6(e). This coefficient informs about the transparency and opacity of the materials. The absorption edges are produced due to electronic transitions from fully occupied valence band to least populated conduction band. The fundamental absorption region is found to be about 2.62, 2.66, 2.51, 2.61, and 2.82 eV for compositions x as 0, 0.25, 0.50, 0.75, and 1, respectively. The value of $\alpha(\omega)$ increases as the photon energy increases, and reach to maximum for energy 16.2, 12.39, 10.95, 8.99, and 8.78 eV for corresponding composition x as 0, 0.25, 0.50, 0.75, and 1. Furthermore, the absorption coefficient decreases as the photon energy increases just after the major peaks. For ZnO, an additional peak is observed at 32.5 eV. The investigated compounds have high absorption coefficients which make them worthy candidates for a wide-range of applications in optics and photovoltaic devices.

The Table 3 summarizes the calculated values of static dielectric constant and refractive index of $ZnO_{1-x}Se_x$ ternary alloys and their endpoints binary compounds ZnO and ZnSe. The results obtained by TB-mBJ and PBE-GGA approximations are compared to other theoretical and experimental studies where a reasonable agreement is observed in between them. The refractive index and dielectric function of $ZnO_{1-x}Se_x$ ternary alloys, their values are increased with increase value of x from 0 to 1. The variations in refractive index and dielectric constant as a function of composition is determined from the quadratic fit which obeys the following expression:

$$n(x)^{\text{TB-mBJ}} = 1.71 + 1.08x - 0.45x^2 \tag{15}$$

$$n(x)^{\text{PBE-GGA}} = 2.16 + 0.98x - 0.44x^2 \tag{16}$$

$$\varepsilon_1(x)^{\text{TB-mBJ}} = 2.93 + 4.03x - 1.48x^2 \tag{17}$$

$$\varepsilon_1(x)^{\text{PBE-GGA}} = 4.68 + 4.51x - 1.90x^2 \tag{18}$$

It is clear that the refractive index and dielectric constant of $ZnO_{1-x}Se_x$ alloys exhibit a non-linear variation with change in x.

TABLE 3: The static dielectric constant with the refractive index of the (WZ) $ZnO_{1-x}Se_x$ ternary alloys.

		This work		Other cal	
$ZnO_{1-x}Se_x$	Parameters	TB-mBJ	PBE-GGA	Theo	Exp
ZnO	$n(\omega=0)$	1.72	2.17	1.71[d], 1.63[e]	1.69[a]
	$\varepsilon_1(\omega=0)$	2.98	4.74	2.91[d], 2.68[e]	2.89[a]
$ZnO_{0.75}Se_{0.25}$	$n(\omega=0)$	1.93	2.36	–	–
	$\varepsilon_1(\omega=0)$	3.75	5.58	–	–
$ZnO_{0.5}Se_{0.5}$	$n(\omega=0)$	2.10	2.52	–	–
	$\varepsilon_1(\omega=0)$	4.43	6.36	–	–
$ZnO_{0.25}Se_{0.75}$	$n(\omega=0)$	2.23	2.61	–	–
	$\varepsilon_1(\omega=0)$	4.97	6.84	–	–
ZnSe	$n(\omega=0)$	2.33	2.69	2.30[f]	2.168[b]
	$\varepsilon_1(\omega=0)$	5.45	7.27	5.66[g]	7.6[c]

[a][43].
[b][44].
[c][45].
[d][46].
[e][47].
[f][48].
[g][49].

Elastic properties

The elastic properties of wurtzite $ZnO_{1-x}Se_x$ alloys and their binary ZnO and ZnSe compounds have been investigated using the IRelast tool which can be employed in Wien2k package [50]. The knowledge of elastic constants C_{ij} gives important information about response of a material to an external applied strain. For hexagonal crystals, there are five independent components of elastic constant tensor: C_{11}, C_{12}, C_{13}, C_{33}, and C_{55}. In order to calculate the elastic constant C_{ij}, we expand the total energy $E(V, \alpha)$ of the crystal into a Taylor series in terms of the distortion parameters [51]:

$$E(V,\delta) = E(V_0,0) + V_0\left(\sum_{i=1}^{6}\tau_i\delta_i + \frac{1}{2}\sum_{i=1}^{6}\sum_{j=1}^{6}C_{ij}\delta_i\delta_j + O(\delta^3)\right) \tag{19}$$

Since, there are five elastic constants, so there will be five different strains [52]. The first distortion can be written as:

$$\begin{pmatrix} 1+\delta & 0 & 0 \\ 0 & 1+\delta & 0 \\ 0 & 0 & 1 \end{pmatrix} \tag{20}$$

It applies a uniform tension in *xy-plane* while keeping the *z-axis* constant. The volume of strain lattice increases, but the symmetry remains hexagonal. The energy for this distortion can be derived by substituting the strain matrix into the energy formula which gives:

$$E(V,\delta) = E(V_0,0) + V_0\delta(\tau_1+\tau_2) + V_0\left((C_{11}+C_{12})\delta^2 + O(\delta^3)\right) \tag{21}$$

The second strain keeps the crystal volume unchanged. The symmetry changes to orthorhombic, and the strain matrix takes the form:

$$\begin{pmatrix} \left(\frac{1+\delta}{1-\delta}\right)^{1/2} & 0 & 0 \\ 0 & \left(\frac{1-\delta}{1+\delta}\right)^{1/2} & 0 \\ 0 & 0 & 1 \end{pmatrix} \tag{22}$$

As a result, Eq. 21 becomes:

$$E(V,\delta) = E(V_0,0) + V_0\left((C_{11} - C_{12})\delta^2 + O(\delta^3)\right) \quad (23)$$

In third strain, the crystal remains hexagonal and tension is applied along the *z-axis*. In this case, the strain matrix can be written as:

$$\begin{pmatrix} 1 & 0 & 0 \\ 0 & 1 & 0 \\ 0 & 0 & 1+\delta \end{pmatrix} \quad (24)$$

Now, the energy Eq. 21 becomes:

$$E(V,\delta) = E(V_0,0) + V_0\delta(\tau_3) + V_0\left((C_{33})\frac{\delta^2}{2} + O(\delta^3)\right) \quad (25)$$

The elastic constant C_{55} can be obtained by applying a deformation that causes the crystal structure transition to triclinic symmetry. The strain matrix is then written as:

$$\begin{pmatrix} 1 & 0 & \delta \\ 0 & 1 & 0 \\ \delta & 0 & 1 \end{pmatrix} \quad (26)$$

where, the Eq. 21 can be rearranged as:

$$E(V,\delta) = E(V_0,0) + V_0\delta(\tau_5) + V_0\left((2C_{55})\delta^2 + O(\delta^3)\right) \quad (27)$$

Finally, in case of fifth strain, the volume remains conserved and hexagonal symmetry of strained lattice is sustained. This situation can be represented by following relation:

$$\begin{pmatrix} (1+\delta)^{-\frac{1}{3}} & 0 & 0 \\ 0 & (1+\delta)^{-\frac{1}{3}} & 0 \\ 0 & 0 & (1+\delta)^{\frac{2}{3}} \end{pmatrix} \quad (28)$$

The energy for this strain can be written as:

$$E(V,\delta) = E(V_0,0) + V_0\left((C_{zz})\frac{\delta^2}{9} + O(\delta^3)\right) \quad (29)$$

whereas, $C_{zz} = C_{11} + C_{12} + 2C_{33} - 4C_{13}$.

When the elastic constants are defined, the other important elastic quantities such as bulk and shear modulus can be determined easily. According to Voigt formula [53], the bulk modulus (B) and the shear modulus (G) are given by the following relations:

$$B_V = \frac{[2(C_{11} + C_{12}) + 4C_{13} + C_{33}]}{9} \quad (30)$$

$$G_V = \frac{M + 12(C_{44} + C_{66})}{30} \quad (31)$$

Here, $M = C_{ZZ} = C_{11} + C_{12} + 2C_{33} - 4C_{13}$ and $C_{66} = \frac{1}{2}(C_{11} - C_{12})$.

From Reuss equation [54], the bulk modulus (B) and shear modulus (G) are written in the form:

$$B_R = \frac{C^2}{M} \quad (32)$$

$$G_R = \frac{5}{2}\frac{C^2 C_{44} C_{66}}{3B_V C_{44} C_{66} + C^2(C_{44} + C_{66})} \quad (33)$$

where, $C^2 = (C_{11} + C_{12})C_{33} - 2C_{13}^2$.

The average values can be given as [55]:

$$B_H = \frac{1}{2}(B_V + B_R) \quad (34)$$

$$G_H = \frac{1}{2}(G_V + G_R) \quad (35)$$

In addition, the Young modulus (E) and Poisson ratio (ν) can also be calculated using the obtained results. These parameters are typically used to determine the hardness of polycrystalline materials. Following equations relate these variables with bulk modulus (B) and the shear modulus (G):

$$E = \frac{9BG}{3B + G} \quad (36)$$

$$\upsilon = \frac{3B - 2G}{2(3B + G)} \quad (37)$$

Table 4 shows the calculated values of elastic constants (C_{11}, C_{12}, C_{13}, C_{33}, and C_{55}), bulk modulus (B), shear modulus (G), Young modulus (E), and Poisson ratio (ν). Due to the absence of theoretical and experimental data for the examined $ZnO_{1-x}Se_x$ ternary alloys, the derived elastic constants can be regarded as good predicted values for future work. The mechanical stability of a hexagonal crystal under isotropic pressure can be evaluated using Born stability criteria [59]:

$$C_{11} > |C_{12}|;\ 2C_{13}^2 < C_{33}(C_{11} + C_{12});\ C_{44} > 0 \quad (38)$$

The obtained results were verified using the above-mentioned equations. The results show that the stability conditions are satisfied and all examined materials are elastically stable in the hexagonal wurtzite structure. In addition, the brittleness and ductility of the materials can be studied using the ratio B/G suggested by Pugh [60]. The ductile materials undergo extensive plastic deformation under external stress, whereas brittle materials undergo minor plastic deformation. Materials with a B/G ratio larger than 1.75, such as ZnO and $ZnO_{0.75}Se_{0.25}$ ($B/G = 1.94$ and 1.87, respectively), are ductile, whereas ZnSe, $ZnO_{0.5}Se_{0.5}$, and $ZnO_{0.25}Se_{0.75}$ are brittle owing to their B/G values which are less than 1.75 ($B/G = 1.67$, 1.55 and 1.63, respectively). Also, the Poisson ratio enables one to estimate the types of bonds in a material. Small Poisson's ratio indicates covalent bonding, and for

metallic bonds, it is approximately 0.33. Whereas for ionic materials, the typical value for v is 0.25 [61]. It can be seen in Table 4 that for all values of x, $ZnO_{1-x}Se_x$ has a Poisson ratio close to 0.25 which indicates a strong ionic bonding in these alloys. These results are also confirmed using the G/B ratio. The metallic materials possess this ratio as 0.4, ionic materials do as 0.6, and covalent materials show as 1.1 [61]. The obtained results are 0.51, 0.54, 0.6, 0.64, and 0.61 for x as 0, 0.25, 0.50, 0.75, and 1, respectively. These values are close to 0.6 which confirms that the investigated alloys are ionic materials.

Conclusions

The structural, electronic, optical and elastic properties of wurtzite binary ZnO, ZnSe compounds and their ternary $ZnO_{1-x}Se_x$ alloys have been investigated using the FP-LAPW method within the framework of DFT. The findings of the study can be summarized as follow:

- The computed lattice parameters of the binary compounds using the WC-GGA method agree well with experimental data.
- The lattice parameters of $ZnO_{1-x}Se_x$ ternary alloys exhibit a small deviation from Vegard's law.
- The $ZnO_{1-x}Se_x$ ternary alloys act as direct bandgap semiconductors.
- The refractive index, reflectivity and absorption coefficient of $ZnO_{1-x}Se_x$ ternary alloys shift toward lower energies with increase in x.
- ZnO and $ZnO_{0.75}Se_{0.25}$ show ductile behavior, whereas the ZnSe, $ZnO_{0.5}Se_{0.5}$, and $ZnO_{0.25}Se_{0.75}$ act as brittle materials.

Method of calculation

In present work, the calculations are carried out using the full potential linearized augmented plane wave (FP-LAPW) within the framework of density functional theory as implemented in Wien2k code [62–64]. The exchange–correlation potential was treated using Wu and Cohen's generalized gradient approximation (WC-GGA) [65]. To improve the accuracy of the energy bandgap measurements, we have used the modified Becke-Johnson potential of Tran-Plaha (TB-mBJ) parameterized by Koller et al. [66], as it has been proven that this approximation is more accurate in calculating the bandgap and hence the optical and electronic properties of the solid materials [67–69]. For comparison, we have also used Perdew-Burke-Ernzerhof's generalized gradient approximation (PBE-GGA) to calculate the electronic and optical properties [70]. In FP-LAPW method, the wave function is expanded into spherical harmonic waves inside non-overlapping muffin-tin spheres. In the remaining space (interstitial region), the wave function developed into a plane wave basis set. The energy convergence criteria are chosen

TABLE 4: Elastic constants (GPa), Bulk modulus B (GPa), Shear modulus G (GPa), Young's modulus E (GPa) and Poisson's ratio υ ratio of the wurtzite $ZnO_{1-x}Se_x$ ternary alloys.

$ZnO_{1-x}Se_x$ alloys		C_{11}	C_{12}	C_{13}	C_{33}	C_{55}	B	G	E	v
ZnO	Pres	293.31	104.24	73.55	278.27	54.63	151.6	78.04	199.84	0.28
	Theo	199.7[d] 201[b]	104.3[d] 124.49[b]	92.9[d] 119.57[b]	192[d] 235.38[b]	43.2[d] 34.73[b]	130.1[d] 151.02[b]	49.8[d]	–	–
	Exp	206[a]	117[a]	118[a]	211[a]	44[a]	–	–	–	–
$ZnO_{0.75}Se_{0.25}$	Pres	205.18	69.56	53.77	234.61	42.66	110.98	59.4	151.23	0.27
	Theo	–	–	–	–	–	–	–	–	–
	Exp	–	–	–	–	–	–	–	–	–
$ZnO_{0.5}Se_{0.5}$	Pres	82	27.24	17.17	90.43	19.08	41.96	25.18	62.95	0.25
	Theo	–	–	–	–	–	–	–	–	–
	Exp	–	–	–	–	–	–	–	–	–
$ZnO_{0.25}Se_{0.75}$	Pres	120.47	34.14	22.28	139.42	27.93	59.73	38.42	94.91	0.24
	Theo	–	–	–	–	–	–	–	–	–
	Exp	–	–	–	–	–	–	–	–	–
ZnSe	Pres	139.58	40.36	29.89	133.5	30.59	68	41.65	103.76	0.25
	Theo	116.9[d] 98.18[c]	37.4[d] 41.44[c]	37.9[d] 29.99[c]	115.3[d] 117.83[c]	28.7[d] 22.57[c]	63.9[d]	34.8[d]	–	–
	Exp	–	–	–	–	–	–	–	–	–

[a][56].

[b][57].

[c][31].

[d][58].

to be 0.0001 *Ry*. The valence wave functions inside muffin-tin spheres are expanded up to l_{max} as 10. In the interstitial region, we have chosen an energy cut-off parameter of the matrix size. The radius of the muffin tin spheres was selected as 1.89, 1.63 and 1.72 atomic units for Zn, O and Se, respectively. A mesh of 100 special *k*-points and 500 special *k*-points is used to, respectively, calculate the structural and optoelectronic properties. The present calculations are based on the Wurtzite (B4) structure, which has hexagonal primitive unit cell with space group P63mc. The binary compound ZnO has two atoms: Zn at (1/3, 2/3, 0) and O at (1/3, 2/3, u). In order to make alloying possible, we considered a supercell of $2 \times 2 \times 1$.Then we substituted the oxygen 'O' atoms by Selenium 'Se' atoms in the $ZnO_{1-x}Se_x$ ternary alloy, we can get series of alloys just by varying the *x* composition from 0 to 1 by step of 0.25.

Acknowledgments

Authors Syed Awais Rouf, Fethi Soyalp and Rabah Khenata are acknowledged for their fruitful discussions and worthful opinions on this work.

Funding

The present work was funded by the Directorate-General for Scientific Research and Technological Development (DGRSDT), Ministry of Higher Education and Scientific Research, Algeria.

Data availability

The datasets generated during and/or analysed during the current study are available from the corresponding author on reasonable request.

Declarations

Conflict of interest The authors disclose any conflict of interest.

Supplementary Information

The online version contains supplementary material available at https://doi.org/10.1557/s43578-022-00864-z.

References

1. H. Bong, W.H. Lee, D.Y. Lee, B.J. Kim, J.H. Cho, K. Cho, High-mobility low-temperature ZnO transistors with low-voltage operation. Appl. Phys. Lett. **96**, 2008–2011 (2010). https://doi.org/10.1063/1.3428357
2. S.I. Inamdar, V.V. Ganbavle, K.Y. Rajpure, ZnO based visible-blind UV photodetector by spray pyrolysis. Superlatt. Microstruct. **76**, 253–263 (2014). https://doi.org/10.1016/j.spmi.2014.09.041
3. J. Dai, C. Xu, X. Xu, J. Guo, J. Li, G. Zhu, Y. Lin, Single ZnO microrod ultraviolet photodetector with high photocurrent gain. ACS Appl. Mater. Interfaces. **5**, 9344–9348 (2013). https://doi.org/10.1021/am403609y
4. J.M. Lin, Y.Z. Zhang, Z.Z. Ye, X.Q. Gu, X.H. Pan, Y.F. Yang, J.G. Lu, H.P. He, B.H. Zhao, Nb-doped ZnO transparent conducting films fabricated by pulsed laser deposition. Appl. Surf. Sci. **255**, 6460–6463 (2009). https://doi.org/10.1016/j.apsusc.2009.01.002
5. K. Matsubara, P. Fons, K. Iwata, A. Yamada, K. Sakurai, H. Tampo, S. Niki, ZnO transparent conducting films deposited by pulsed laser deposition for solar cell applications. Thin Solid Films **431–432**, 369–372 (2003). https://doi.org/10.1016/S0040-6090(03)00243-8
6. Y. Li, Y. Men, X. Kong, Z. Gao, L. Han, X. Li, Enhanced electrical properties of ZnO transparent conducting films prepared by electron beam annealing. Appl. Surf. Sci. **428**, 191–198 (2018). https://doi.org/10.1016/j.apsusc.2017.09.063
7. J.H. Lee, K.H. Ko, B.O. Park, Electrical and optical properties of ZnO transparent conducting films by the sol-gel method. J. Cryst. Growth. **247**, 119–125 (2003). https://doi.org/10.1016/S0022-0248(02)01907-3
8. Y. Ryu, T.S. Lee, J.A. Lubguban, H.W. White, B.J. Kim, Y.S. Park, C.J. Youn, Next generation of oxide photonic devices: ZnO-based ultraviolet light emitting diodes. Appl. Phys. Lett. (2006). https://doi.org/10.1063/1.2210452
9. S. Liang, H. Sheng, Y. Liu, Z. Huo, Y. Lu, H. Shen, ZnO Schottky ultraviolet photodetectors. J. Cryst. Growth. **225**, 110–113 (2001). https://doi.org/10.1016/S0022-0248(01)00830-2
10. C. Liu, J.A. Zapien, Y. Yao, X. Meng, C.S. Lee, S. Fan, Y. Lifshitz, S.T. Lee, High-density, ordered ultraviolet light-emitting ZnO nanowire arrays. Adv. Mater. **15**, 838–841 (2003). https://doi.org/10.1002/adma.200304430
11. T. Makino, Y. Segawa, M. Kawasaki, A. Ohtomo, R. Shiroki, K. Tamura, T. Yasuda, H. Koinuma, Band gap engineering based on $Mg_xZn_{1-x}O$ and $Cd_yZn_{1-y}O$ ternary alloy films. Appl. Phys. Lett. **78**, 1237–1239 (2001). https://doi.org/10.1063/1.1350632
12. S. Choopun, R.D. Vispute, W. Yang, R.P. Sharma, T. Venkatesan, H. Shen, Realization of band gap above 5.0 eV in metastable cubic-phase $Mg_xZn_{1-x}O$ alloy films. Appl. Phys. Lett. **80**, 1529–1531 (2002). https://doi.org/10.1063/1.1456266
13. K. Sakurai, T. Takagi, T. Kubo, D. Kajita, T. Tanabe, H. Takasu, S. Fujita, S. Fujita, Spatial composition fluctuations in blue-luminescent ZnCdO semiconductor films grown by molecular beam epitaxy. J. Cryst. Growth. **237–239**, 514–517 (2002). https://doi.org/10.1016/S0022-0248(01)01954-6
14. M. Rashid, F. Hussain, M. Imran, S.A. Ahmad, N.A. Noor, M.U. Sohaib, S.M. Alay-E-Abbas, Structural, electronic, and optical properties of $ZnO_{1-x}Se_x$ alloys using first-principles calculations. Chin Phys. B. (2013). https://doi.org/10.1088/1674-1056/22/8/087301

15. G. Baldissera, C. Persson, Understanding the optical properties of $ZnO_{1-x}S_x$ and ZnO1-xSex alloys, J. Appl. Phys. 119 (2016). https://doi.org/10.1063/1.4940700.
16. R. Manotum, R. Klinkla, N. Phaisangittisakul, U. Pinsook, T. Bovornratanaraks, Effect of pressure on the stability and electronic structure of $ZnO_{0.5}S_{0.5}$ and $ZnO_{0.5}Se_{0.5}$. J. Electron. Mater. **46**, 6856–6863 (2017). https://doi.org/10.1007/s11664-017-5708-1
17. K. Iwata, A. Yamada, P. Fons, K. Matsubara, S. Niki, Natural ordering of $ZnO_{1-x}Se_x$ grown by radical source MBE. J. Cryst. Growth. **251**, 633–637 (2003). https://doi.org/10.1016/S0022-0248(02)02206-6
18. K. Iwata, P. Fons, A. Yamada, H. Shibata, K. Matsubara, K. Nakahara, H. Takasu, S. Niki, Bandgap engineering of ZnO using Se. Phys. Status Solidi Basic Res. **229**, 887–890 (2002). https://doi.org/10.1002/1521-3951(200201)229:2%3c887::AID-PSSB887%3e3.0.CO;2-G
19. J.C. Lee, J.E. Lee, J.W. Lee, J.C. Lee, N.G. Subramaniam, T.W. Kang, R. Ahuja, Se concentration dependent band gap engineering in $ZnO_{1-x}Se_x$ thin film for optoelectronic applications. J. Alloys Compd. **585**, 94–97 (2014). https://doi.org/10.1016/j.jallcom.2013.09.134
20. M.A. Mayer, D.T. Speaks, K.M. Yu, S.S. Mao, E.E. Haller, W. Walukiewicz, Band structure engineering of ZnO_{1-x} Sex alloys. Appl. Phys. Lett. **97**, 2010–2013 (2010). https://doi.org/10.1063/1.3464323
21. M.A. Mayer, K.M. Yu, E.E. Haller, W. Walukiewicz, Tuning structural, electrical, and optical properties of oxide alloys: $ZnO_{1-x}Se_x$. J. Appl. Phys. (2012). https://doi.org/10.1063/1.4724336
22. M. Welna, R. Kudrawiec, Y. Nabetani, W. Walukiewicz, Band anticrossing in ZnOSe highly mismatched alloy. Appl. Phys. Express. (2014). https://doi.org/10.7567/APEX.7.071202
23. M. Welna, M. Baranowski, W.M. Linhart, R. Kudrawiec, K.M. Yu, M. Mayer, W. Walukiewicz, Multicolor emission from intermediate band semiconductor $ZnO_{1-x}Se_x$. Sci. Rep. **7**, 3–8 (2017). https://doi.org/10.1038/srep44214
24. F.D. Murnaghan, The compressibility of media under extreme pressures. Proc. Natl. Acad. Sci. **30**, 244–247 (1944). https://doi.org/10.1073/pnas.30.9.244
25. N. Tit, S. Dagher, A. Ayesh, Y. Haik, Bowing character in wurtzite ZnO-based ternary alloys. J. Electron. Mater. **41**, 3111–3118 (2012). https://doi.org/10.1007/s11664-012-2188-1
26. H. Karzel, W. Potzel, M. Köfferlein, W. Schiessl, M. Steiner, U. Hiller, G. Kalvius, D. Mitchell, T. Das, Lattice dynamics and hyperfine interactions in ZnO and ZnSe at high external pressures. Phys. Rev. B **53**, 11425–11438 (1996). https://doi.org/10.1103/PhysRevB.53.11425
27. F. Decremps, F. Datchi, M. Saitta, A. Polian, S. Pascarelli, A. Di Cicco, P. Itié, F. Baudelet, Local structure of condensed zinc oxide. Phys. Rev. B **68**, 1–10 (2003). https://doi.org/10.1103/PhysRevB.68.104101
28. A. Djelal, K. Chaibi, N. Tari, K. Zitouni, A. Kadri, Ab-initio DFT-FP-LAPW/TB-mBJ/LDA-GGA investigation of structural and electronic properties of $Mg_xZn_{1-x}O$ alloys in Würtzite, rocksalt and zinc-blende phases. Superlattices Microstruct. **109**, 81–98 (2017). https://doi.org/10.1016/j.spmi.2017.04.041
29. R. John, S. Padmavathi, Ab initio calculations on structural, electronic and optical properties of ZnO in Wurtzite phase. Cryst. Struct. Theory Appl. **05**, 24–41 (2016). https://doi.org/10.4236/csta.2016.52003
30. O. Zakharov, A. Rubio, X. Blase, M.L. Cohen, S.G. Louie, Quasiparticle band structures of six II-VI compounds: ZnS, ZnSe, ZnTe, CdS, CdSe, and CdTe. Phys. Rev. B. **50**, 10780–10787 (1994). https://doi.org/10.1103/PhysRevB.50.10780
31. S. Ferahtia, S. Saib, N. Bouarissa, S. Benyettou, Structural parameters, elastic properties and piezoelectric constants of wurtzite ZnS and ZnSe under pressure. Superlattices Microstruct. **67**, 88–96 (2014). https://doi.org/10.1016/j.spmi.2013.12.021
32. S.Z. Karazhanov, P. Ravindran, A. Kjekshus, H. Fjellvåg, B.G. Svensson, Electronic structure and optical properties of ZnX (X=O, S, Se, Te): a density functional study. Phys. Rev. B. **75**, 1–14 (2007). https://doi.org/10.1103/PhysRevB.75.155104
33. L. Vegard, Die Konstitution der Mischkristalle und die Raumfüllung der Atome. Z. Phys. **5**, 17–26 (1921). https://doi.org/10.1007/BF01349680
34. A. Mang, K. Reimann, S. Rübenacke, Band gaps, crystal-field splitting, spin-orbit coupling, and exciton binding energies in ZnO under hydrostatic pressure. Solid State Commun. **94**, 251–254 (1995). https://doi.org/10.1016/0038-1098(95)00054-2
35. A. Ebina, E. Fukunaga, T. Takahashi, Variation with composition of the E0 and E0 + 0 gaps in ZnS_xSe_{1-x} alloys. Phys. Rev. B. **10**, 2495–2500 (1974). https://doi.org/10.1103/PhysRevB.10.2495
36. R. Kudrawiec, W. Walukiewicz, Electromodulation spectroscopy of highly mismatched alloys. J. Appl. Phys. **126**, 1–30 (2019). https://doi.org/10.1063/1.5111965
37. A. Belabbes, A. Zaoui, M. Ferhat, Lattice mismatch consequences for the intrinsic characteristics in the dilute (Zn, Se)O alloys. J. Phys. **19**, 1–6 (2007). https://doi.org/10.1088/0953-8984/19/45/456212
38. M. Sargolzaei, N. Lotfizadeh, R. Hayn, First principles study on magnetic properties of Zn vacancies in ZnO doped with single chalcogen X (X=S, Se, and Te). J. Appl. Phys. **109**, 1–6 (2011). https://doi.org/10.1063/1.3562168?ver=pdfcov
39. R.T. Girard, O. Tdjernberg, G. Chiaia, S. Söderholm, U.O. Karlsson, C. Wigren, H. Nylèn, I. Lindau, Electronic structure of ZnO (0001) studied by angel-resolved photoelectron spectroscopy. Surf. Sci. **373**, 409–417 (1997). https://doi.org/10.1016/S0039-6028(96)01181-8
40. C. Ambrosch-Draxl, J.O. Sofo, Linear optical properties of solids within the full-potential linearized augmented planewave method. Comput. Phys. Commun. **175**, 1–14 (2006). https://doi.org/10.1016/j.cpc.2006.03.005

41. M. O'Donnell, E.T. Jaynes, J.G. Miller, Kramers-Kronig relationship between ultrasonic attenuation and phase velocity. J. Acoust. Soc. Am. **69**, 696–701 (1981). https://doi.org/10.1121/1.385566
42. M. Fox, *Optical Properties of Solids* (Oxford University Press, First edit, 2001)
43. D. Komaraiah, E. Radha, Y. Vijayakumar, J. Sivakumar, M.V.R. Reddy, R. Sayanna, Optical, structural and morphological properties of photocatalytic ZnO thin films deposited by pray pyrolysis technique. Mod. Res. Catal. **05**, 130–146 (2016). https://doi.org/10.4236/mrc.2016.54011
44. M.F. Hasaneen, Z.A. Alrowaili, W.S. Mohamed, Structure and optical properties of polycrystalline ZnSe thin films: validity of Swanepol's approach for calculating the optical parameters. Mater. Res. Express. (2020). https://doi.org/10.1088/2053-1591/ab6779
45. T. Hattori, Y. Homma, A. Mitsuishi, M. Tacke, Indices of refraction of ZnS, ZnSe, ZnTe, CdS, and CdTe in the far infrared. Opt. Commun. **7**, 229–232 (1973). https://doi.org/10.1016/0030-4018(73)90015-1
46. A. Baizid, A. Mokadem, A. Ouerdane, M. Guezzoul, M. Bouslama, H. Benchenane, B. Kharroubi, M. Bedrouni, M. Abdelkrim, K.B. Bensassi, M.S. Halati, First principles calculation of structural, electronic and optical properties of K-doped ZnO. Comput. Condens. Matter. **27**, e00558 (2021). https://doi.org/10.1016/j.cocom.2021.e00558
47. S. Shabbir, A. Shaari, B. Ul-Haq, R. Ahmed, M. Ahmed, Investigations of novel polymorphs of ZnO for optoelectronic applications. Optik (Stuttg). **206**, 164285 (2020). https://doi.org/10.1016/j.ijleo.2020.164285
48. S. Hussain, L. Guo, H. Louis, S. Zhu, T. He, First-principles calculations of wurtzite $ZnS_{1-x}Se_x$ solid solutions for photocatalysis. Mater. Today Commun. **21**, 1–9 (2019). https://doi.org/10.1016/j.mtcomm.2019.100672
49. W. Benstaali, S. Bentata, A. Abbad, A. Belaidi, Ab-initio study of magnetic, electronic and optical properties of ZnSe doped-transition metals. Mater. Sci. Semicond. Process. **16**, 231–237 (2013). https://doi.org/10.1016/j.mssp.2012.10.001
50. M. Jamal, Hex-elastic, (2013). http://www.wien2k.at/reg_user/unsupported/cubic-elast/guide-Hex.pdf.
51. L. Landau, Theory of Elasticity, Third Edit, Elsevier, Amsterdam (1986). https://doi.org/10.1016/C2009-0-25521-8.
52. L. Fast, J.M. Wills, B. Johansson, O. Eriksson, Elastic constants of hexagonal transition metals: Theory. Phys. Rev. B. **51**, 17431–17438 (1995). https://doi.org/10.1103/PhysRevB.51.17431
53. W. Voigt, Lehrbuch der Kristallphysik, Vieweg+Teubner Verlag. Wiesbaden (1966). https://doi.org/10.1007/978-3-663-15884-4
54. A. Reuss, Berechnung der Fließgrenze von Mischkristallen auf Grund der Plastizitätsbedingung für Einkristalle. ZAMM J. Appl. Math. Mech./Z. Angew. Math. Mech. **9**, 49–58 (1929). https://doi.org/10.1002/zamm.19290090104
55. R. Hill, The elastic behaviour of a crystalline aggregate. Proc. Phys. Soc. Sect. A. **65**, 349–354 (1952). https://doi.org/10.1088/0370-1298/65/5/307
56. G. Carlotti, D. Fioretto, G. Socino, E. Verona, Brillouin scattering determination of the whole set of elastic constants of a single transparent film of hexagonal symmetry. J. Phys. Condens. Matter. **7**, 9147–9153 (1995). https://doi.org/10.1088/0953-8984/7/48/006
57. F. Wang, J. Wu, C. Xia, C. Hu, C. Hu, P. Zhou, L. Shi, Y. Ji, Z. Zheng, X. Liu, Thermodynamic and elastic properties of hexagonal ZnO under high temperature. J. Alloys Compd. **597**, 50–57 (2014). https://doi.org/10.1016/j.jallcom.2013.12.212
58. L.A. Valdez, M.A. Caravaca, R.A. Casali, Ab-initio study of elastic anisotropy, hardness and volumetric thermal expansion coefficient of ZnO, ZnS, ZnSe in wurtzite and zinc blende phases. J. Phys. Chem. Solids. **134**, 245–254 (2019). https://doi.org/10.1016/j.jpcs.2019.05.019
59. M. Born, H. Kuang, *Dynamical Theory of Crystal Lattices, First edition* (Oxford University Press, Oxford, 1954)
60. S.F. Pugh, XCII. Relations between the elastic moduli and the plastic properties of polycrystalline pure metals, London, Edinburgh, Dublin Philos. Mag. J. Sci. 45 (1954) 823–843. https://doi.org/10.1080/14786440808520496.
61. J. Haines, J.M. Légar, G. Bocquillon, Synthesis and design of superhard materials. Annu. Rev. Mater. Res. **31**, 1–23 (2001). https://doi.org/10.1146/annurev.matsci.31.1.1
62. P. Blaha, K. Schwarz, P. Sorantin, S.B. Trickey, Full-potential, linearized augmented plane wave programs for crystalline systems. Comput. Phys. Commun. **59**, 399–415 (1990). https://doi.org/10.1016/0010-4655(90)90187-6
63. K. Schwarz, P. Blaha, Solid state calculations using WIEN2k. Comput. Mater. Sci. **28**, 259–273 (2003). https://doi.org/10.1016/S0927-0256(03)00112-5
64. P. Blaha, K. Schwarz, F. Tran, R. Laskowski, G.K.H. Madsen, L.D. Marks, WIEN2k: an APW+lo program for calculating the properties of solids. J. Chem. Phys. (2020). https://doi.org/10.1063/1.5143061
65. Z. Wu, R.E. Cohen, More accurate generalized gradient approximation for solids. Phys. Rev. B Condens. Matter Mater. Phys. **73**, 2–7 (2006). https://doi.org/10.1103/PhysRevB.73.235116
66. F. Tran, P. Blaha, Accurate band gaps of semiconductors and insulators with a semilocal exchange-correlation potential. Phys. Rev. Lett. **102**, 5–8 (2009). https://doi.org/10.1103/PhysRevLett.102.226401
67. R. Moussa, A. Abdiche, R. Khenata, X.T. Wang, D. Varshney, X.W. Sun, S. Bin Omran, A. Bouhemadou, D.P. Rai, Structural, electronic, optical, thermodynamic and elastic properties of the zinc-blende AlxIn1-xN ternary alloys: a first principles calculations. J. Phys. Chem. Solids. **119**, 36–49 (2018). https://doi.org/10.1016/j.jpcs.2018.03.035

68. R. Moussa, A. Abdiche, R. Khenata, F. Soyalp, First principles calculation of the structural, electronic, optical and elastic properties of the cubic $Al_xGa_{1-x}Sb$ ternary alloy. Opt. Mater. Amst. **113**, 110850 (2021). https://doi.org/10.1016/j.optmat.2021.110850
69. R. Moussa, A. Abdiche, R. Khenata, R. Ahmed, S.A. Tahir, S. Bin Omran, A. Bouhemadou, Investigation of the structural, electronic, optical, elastic, and thermodynamic properties of the zinc blende Ga1-xAlxAs1-yPy quaternary alloys: a DFT-Based simulation. Mater. Sci. Semicond. Process. **126**, 105642 (2021). https://doi.org/10.1016/j.mssp.2020.105642
70. J.P. Perdew, K. Burke, M. Ernzerhof, Generalized gradient approximation made simple. Phys. Rev. Lett. **77**, 3865–3868 (1996). https://doi.org/10.1103/PhysRevLett.77.3865